Lattice vibrations of $Si_{1-x}C_x$ epilayers on Si(100)

D. J. Lockwood, H. X. Xu,* and J.-M. Baribeau
Institute for Microstructural Sciences, National Research Council, Ottawa, Ontario, Canada K1A 0R6
(Received 11 February 2003; published 16 September 2003)

Raman spectroscopy has been used to investigate the lattice vibrations of $Si_{1-x}C_x$ ($0<x<0.02$) epilayers grown on Si(100) by electron cyclotron resonance plasma-assisted molecular beam epitaxy. Spectral contributions due to first- and second-order longitudinal and transverse optic phonons together with disorder-induced features have been evaluated by a detailed polarization and C concentration dependence analysis. The band parameters exhibit generally a linear dependence on x. A Raman line observed near 630 cm^{-1}, which in past work has been associated with C ordering in the Si lattice, is found not to agree with this interpretation. It is associated with interstitial C. The optical absorption coefficient near 458 nm is deduced from the Raman intensity information, and is found to increase significantly with increasing x.

DOI: 10.1103/PhysRevB.68.115308 PACS number(s): 78.30.Ly, 78.30.Am, 78.20.Ci, 63.20.Pw

I. INTRODUCTION

The growth of pseudomorphic layers of $Si_{1-x}C_x$ on Si has received considerable attention in recent years, because of the hope of achieving a larger band gap and also for achieving strain compensation by incorporating C in $Si_{1-y}Ge_y$ alloys grown on Si. Silicon and Ge are miscible over the entire composition range, but C has a low solubility in Si and prefers to form SiC at higher substrate temperatures. Nevertheless, growth techniques, such as molecular beam epitaxy (MBE) and low-temperature chemical vapor deposition (CVD), which are regulated by surface kinetics, have been remarkably successful in growing high-quality expitaxial films of $Si_{1-x}C_x$ and $Si_{1-x-y}C_xGe_y$ for concentrations up to $x\approx0.02$. The structural and electronic properties of $Si_{1-x}C_x$ and $Si_{1-x-y}C_xGe_y$ have been well researched, but their optical and vibrational characteristics are less well known.[1]

Carbon, being a much smaller atom than Si, produces not only a tensile strain in $Si_{1-x}C_x$ alloys lattice matched to Si but also a localized distortion of the regular Si lattice owing to the shorter Si-C bond length.[2,3] Raman spectroscopy has been shown to be a valuable technique for evaluating strain in the $Si_{1-y}Ge_y$ system,[4,5] because the optical phonon frequencies of the alloy are sensitive to strain. A few Raman investigations have been made in an analogous way of strain in the $Si_{1-x}C_x$ system and these have also revealed the local deformation by C of the Si lattice,[6–8] but most of the phonon work has concentrated on the $Si_{1-x-y}C_xGe_y$ system where there have been numerous studies (see, for example, Refs. 3, 8, and 9–16). This earlier Raman work on $Si_{1-x}C_x$ revealed first-order Raman bands at 605 and 475 cm^{-1} that were assigned to the local mode of C in Si (Ref. 17) (seen also in the infrared[18–20]) and lattice relaxation around the substitutional C atoms in Si,[6–8] respectively. Weak second-order Raman scattering from the C local mode was also observed at around 1200 cm^{-1}.[6] In addition, a weak band at 625 cm^{-1} was observed as a shoulder to the 605 cm^{-1} line,[7,8] which was attributed to pairs of C atoms at third-nearest-neighbor lattice sites.[8,21] Surprisingly, despite the widespread interest in the physics of this disordered system, no systematic study of the concentration dependence of the Raman modes of $Si_{1-x}C_x$ has been undertaken. This is possibly because interest had turned to $Si_{1-x-y}C_xGe_y$, where detailed experimental and theoretical studies of the first-order phonons have been undertaken.[3,8]

Here we present a detailed investigation of the entire polarized Raman spectrum of $Si_{1-x}C_x$ for C concentrations $x<0.02$ and report the concentration dependence of the band parameters for peaks due to first-order, second-order, and disorder-induced scattering. The observed features and their concentration dependencies are related to earlier experimental and theoretical work.

II. EXPERIMENT

A. Epilayer growth and characterization

The epitaxy was performed on a VG V80 Si MBE system equipped with electron beam evaporators for Si and Ge using a methodology described previously.[22,23] Prime grade lightly doped (001) Si wafers were prepared by a 600 s exposure to ultraviolet light (UV ozone reactor) to photochemically remove surface hydrocarbon contamination, and then immersed for 30 s in a 5% HF aqueous solution to remove the native oxide and hydrogen passivate the surface. The wafer was then immediately introduced into the MBE system. After thermal desorption of the surface hydrogen, an epitaxial Si buffer (typically 100 nm thick) was grown prior to the alloy deposition.

The carbon source used in this work is a Wavemat MPDR 610i electron cyclotron resonance (ECR) plasma source. Details of the source are described elsewhere.[23] For these growths, an approximately 10:1 high purity argon/methane gas mixture was supplied to the source. The ECR source was typically operated at a gas flow of 2 sccm and 100 W of 2.45 GHz microwave radiation. Under those conditions the pressure in the deposition chamber was typically 1.5×10^{-5} T. In addition to Ar and CH_4 related peaks (in a 20:1 ratio) residual gas analysis revealed hydrogen and water peaks at a level $\sim0.1\%$ of the Ar signal and a peak at mass 28 (CO/N_2 combination) at 0.01%. Any oxygen was below the detection limit of the mass spectrometer.

Various $Si/Si_{1-x}C_x$ single heterostructures were prepared. The films were typically grown at a rate of 0.1 to 0.2 nm s^{-1}

TABLE I. $Si_{1-x}C_x$ epilayer sample parameters, as determined by x-ray diffraction.

C fraction (%)	Epilayer thickness (nm)	Si cap thickness (nm)
0.29	198.0	
0.39	226.2	
0.40	240.6	136.8
0.40	236.5	
0.44	206.8	
0.60	217.2	141.6
0.65	191.0	
0.76	112.3	
0.83	124.6	
0.89	230.4	142.2
0.90	170.4	
0.93	162.5	
1.06	115.7	120.4
1.71	88.5	

at a temperature of 525 °C. The properties of films grown under various gas flows (1–8 sccm range), powers (25–200 W range), deposition rates (0.1–0.5 nm s^{-1}), and temperatures (450–650 °C range) were also studied and are discussed elsewhere.[23]

The chemical composition of the various samples was measured by secondary ion mass spectrometry (SIMS) with a Cameca $4f$ instrument using a cesium beam. Carbon concentrations were calibrated against ion implanted standards. The structural parameters and crystal perfection were assessed by high-resolution x-ray diffraction (HRXRD) using a Philips MRD system in the (400) geometry. Rocking curves were analyzed with an automated algorithm based on the dynamical theory of diffraction[24] using the approximation of Kelires[25] for the composition dependence of the $Si_{1-x}C_x$ lattice constant. The layer thicknesses and (substitutional) C composition were determined by dynamical simulations of (400) x-ray diffraction rocking curves. Excellent fits were obtained on all samples. The thickness accuracy is of the order of 0.5 nm. The resultant sample parameters are given in Table I.

X-ray diffraction is mostly sensitive to the distribution of atomic species on lattice sites and not to atoms sitting on interstitial or defect sites. Figure 1 compares the C concentration as measured by SIMS to the substitutional concentration as determined by HRXD for the $Si_{1-x}C_x$ epilayers studied here. Up to a concentration of about 1%, a one to one relationship between these quantities (see Fig. 1) indicates that C atoms predominantly occupy substitutional sites. For higher C concentrations, the deviation from a linear relationship indicates that more and more C atoms sit on nonsubstitutional sites.

B. Raman spectroscopy

The Raman scattering spectra of samples immersed in He gas at room temperature (295 K) were excited in a quasi-backscattering geometry[26] with 200 mW of argon laser light at 457.9 nm, measured with a Spex 14108 double monochromator, and detected with a cooled RCA 31034A photomultiplier. The incident light was polarized in the scattering plane and the scattered light was recorded with and without polarization analysis, i.e., in $x(y'z')\bar{x}$ and $x(y'y'+y'z')\bar{x}$ polarizations, respectively, with x along [100], y' along [011], and z' along $[0\bar{1}1]$.[26]

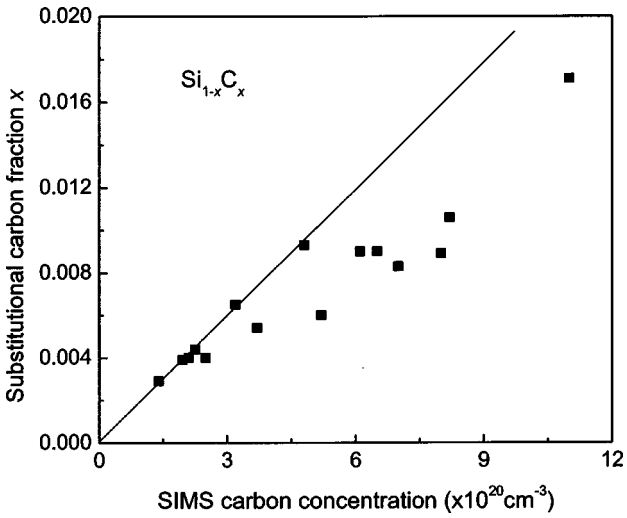

FIG. 1. Comparison of the C concentration in $Si_{1-x}C_x$ epilayers, as determined separately by SIMS and HRXD.

III. RAMAN SPECTRA

Representative unanalyzed and polarized Raman spectra for a sample with $x=0.0171$ (note that from now on all x values quoted are those obtained from HRXRD analysis) are compared with those of crystalline Si in Fig. 2. Weak Raman peaks due to the $Si_{1-x}C_x$ layer are seen to extend up to 1200 cm^{-1}: No other peaks were detected at higher frequencies. The alloy spectrum is mostly dominated by the first- (at 520 cm^{-1}) and second-order Raman spectrum of Si, which arises from the underlying Si buffer layer plus Si substrate and also, for some samples, a 40–140 nm thick Si cap. By a least-squares peak fitting procedure, the integrated intensity of the 520 cm^{-1} Si optical phonon line was obtained for each alloy sample and for the Si reference spectrum. By scaling the intensity of the Si spectrum using the 520 cm^{-1} line intensity ratio thus obtained, the Si spectral features were subtracted from the measured alloy spectra to reveal the "bare" $Si_{1-x}C_x$ epilayer spectrum.

Some results from such subtractions, covering the $0<x<0.02$ concentration range, are shown in Fig. 3. These spectra clearly reveal the numerous Raman features exhibited by the $Si_{1-x}C_x$ epilayers (the sharp discontinuities around 520 cm^{-1} are artifacts of the subtraction process).

Raman selection rules for cubic symmetry indicate that in true backscattering only longitudinal optical (LO) phonons can be observed and will appear in $x(y'y')\bar{x}$ polarization. Raman scattering from transverse optical (TO) phonons, which would appear in $x(y'z')\bar{x}$ polarization, is forbidden.

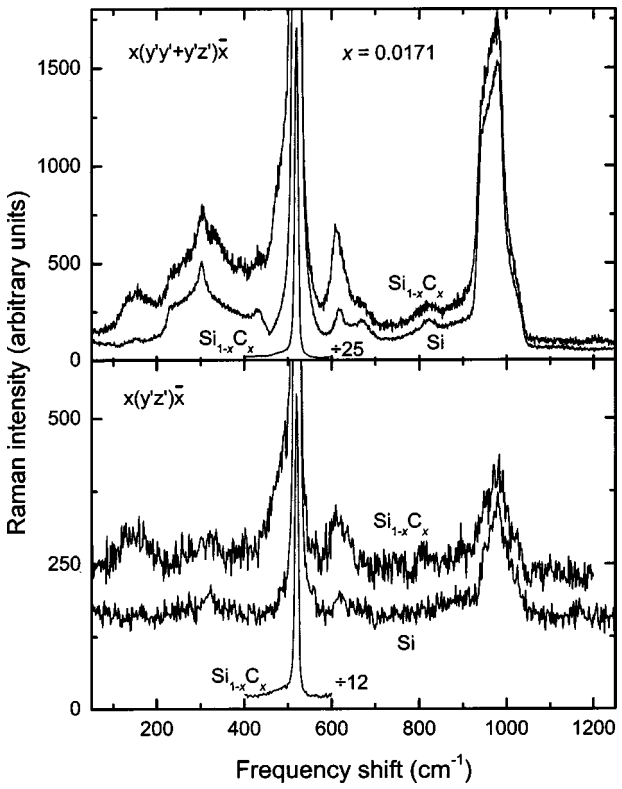

FIG. 2. Room temperature Raman spectrum of $Si_{1-x}C_x$ ($x=0.171$) grown on Si(100) compared with that of Si(100) recorded in $x(y'y'+y'z')\bar{x}$ and $x(y'z')\bar{x}$ polarizations at a resolution of 7.8 cm^{-1}.

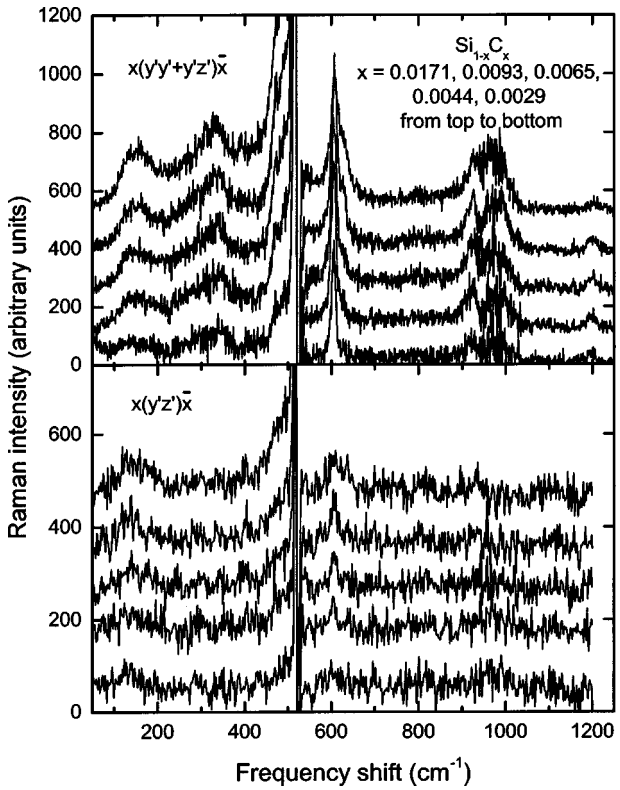

FIG. 3. $Si_{1-x}C_x$ Raman spectra after substration of the Si(100) substrate spectrum in $x(y'y'+y'z')\bar{x}$ and $x(y'z')\bar{x}$ polarizations.

In our quasibackscattering experiments, the scattering angle within the sample is a few degrees off true backscattering[26] allowing the TO modes to be observed. Thus the TO modes for the alloy are evident in $x(y'z')\bar{x}$ polarization in Fig. 3, and are very weak, as expected On the other hand, the LO modes are still very strong by comparison and dominate the unanalysed $x(y'y'+y'z')\bar{x}$ spectra shown in Fig. 3. In the analysis of the Raman spectra that follows, the very weak TO contribution within the unanalysed spectra is ignored.

IV. ANALYSIS OF RAMAN SPECTRA

The Raman spectrum of each sample was analyzed in regions using a least-squares peak fitting procedure to obtain the Lorentzian-model line parameters of frequency, linewidth (FWHM), and integrated intensity for each feature. The resulting integrated intensity was then normalized to unit layer thickness to correct for the variation in the sample layer thicknesses. The results obtained for each region will be presented and discussed in turn.

A. First-order modes—600 cm^{-1} region

The results of fits to several samples in the 600 cm^{-1} frequency region are shown in Fig. 4 for $x(y'y'+y'z')\bar{x}$ polarization. A sharp and well-defined feature is evident at about 605 cm^{-1} together with a sideband at about 630 cm^{-1}. Similar results were obtained in $x(y'z')\bar{x}$ polarization. The C concentration dependencies of the band parameters obtained from the fits for both polarizations are given in Fig. 5. The straight lines shown in this figure are the results of error-bar-weighted least-squares fits to the various data sets for each band parameter and for each polarization.

By analogy with $Si_{1-y}Ge_y$, which exhibits a three mode behavior (see, e.g., Refs. 27 and 28)—the so called Si-Si, Si-Ge, and Ge-Ge modes—$Si_{1-x}C_x$ can also be expected to exhibit three types of modes: Si-Si, Si-C, and C-C. The Si-Si modes can be expected near 520 cm^{-1} (Si), while the C-C modes could be as high as 1332 cm^{-1} (diamond). The dominant 605 cm^{-1} band in this frequency region, which is due to C substituting for Si on the diamond lattice sites,[17] corresponds to a Si-C mode of vibration. The linear fit to the data shown in Fig. 5 for $x(y'y'+y'z')\bar{x}$ polarization gives

$$\omega_{\mathrm{LO}}^{\mathrm{Si\text{-}C}}(\mathrm{cm}^{-1}) = 604.5(\pm 0.2) + 258.4(\pm 35.7)x. \qquad (1)$$

The quantities in parentheses are the standard deviations of the fitting parameters. The best fit in $x(y'z')\bar{x}$ polarization is

$$\omega_{\mathrm{TO}}^{\mathrm{Si\text{-}C}}(\mathrm{cm}^{-1}) = 603.5(\pm 1.3) + 222.3(\pm 175.6)x. \qquad (2)$$

This result and the data in Fig. 5 indicate a slight, but consistent, difference in frequency (~ 1 cm^{-1}) between the LO and TO modes. Normally, in bulk elemental semiconductors having the cubic diamond structure, there is no LO-TO splitting at the Brillouin zone center. The observation of a small splitting here suggests a lowering of the symmetry as a consequence of tensile strain imposed during growth of the epilayer. In the limit as $x \to 0$, Eq. (1) indicates that the fre-

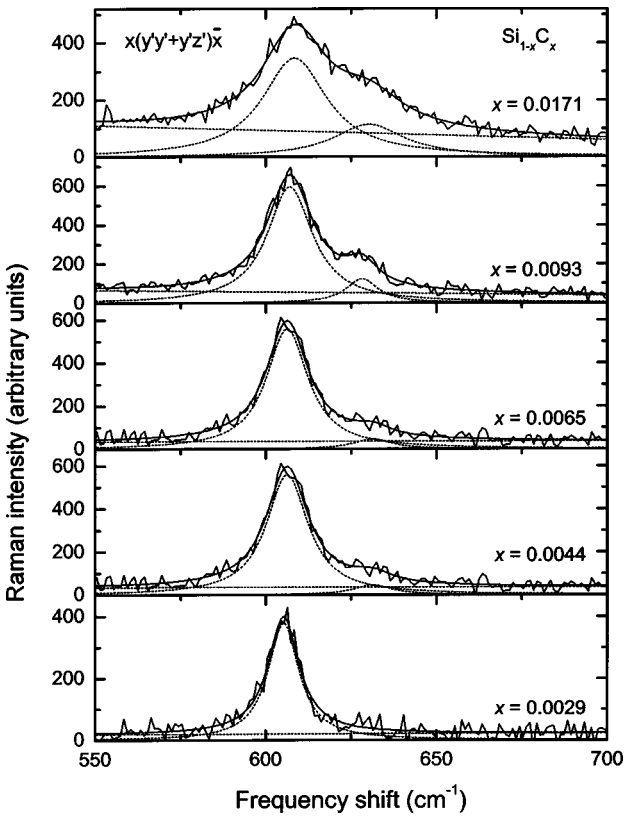

FIG. 4. Curve-resolved $Si_{1-x}C_x$ Raman spectra in $x(y'y'+y'z')\bar{x}$ polarization. The solid line is the fit to the data, while the dashed lines show the two component bands (Si-C and satellite) and background.

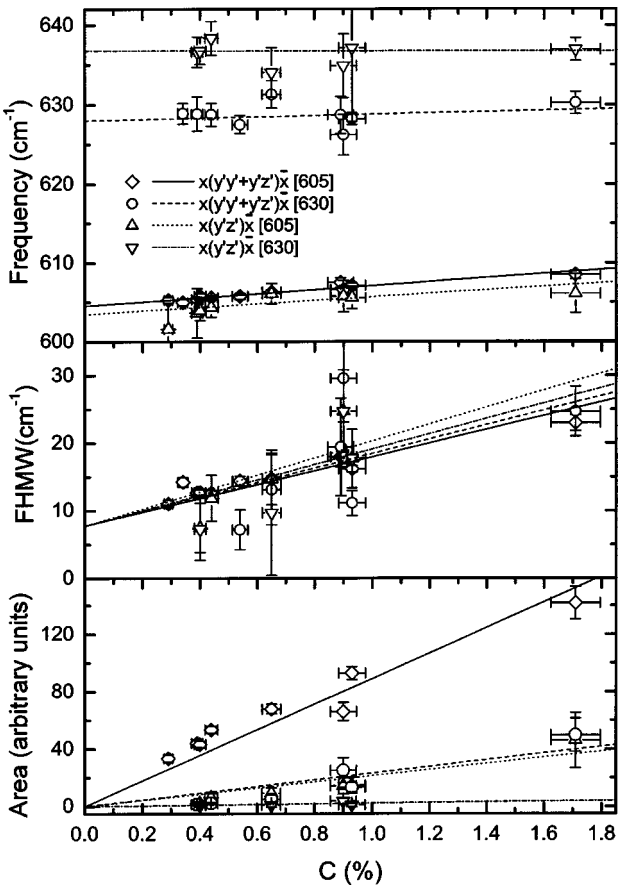

FIG. 5. Concentration dependence of the band parameters of frequency, full width at half maximum (FWHM), and integrated intensity for the Si-C Raman line and its satellite. The straight lines are the results of error-bar-weighted least squares fits to the data.

quency of the localized mode of an isolated C atom in Si is $604.5 \pm 0.2\ \mathrm{cm}^{-1}$, which is in good agreement with the earlier measurements by infrared[19,29] and Raman[6,17] spectroscopy. The variation in frequency with concentration [Eq. (1)] for the Si-C mode in $Si_{1-x}C_x$ has not been published before. However, in the $Si_{1-x-y}C_xGe_y$ system, Finkman *et al.*[14,16] found $\omega^{\text{Si-C}}_{\text{SiCGe}}(\mathrm{cm}^{-1}) = 605.6 + 276x$ for $y = 0.1$, while Guedj *et al.*[15] report a mode shift of $370x$ for $y = 0.1$. The Finkman *et al.* result is in satisfactory agreement with our Eq. (1).

The frequency of the peak near $630\ \mathrm{cm}^{-1}$ exhibits a much weaker concentration dependence (essentially none) than the Si-C mode over the same concentration range. The least-squares fit to the data shown in Fig. 5 yielded

$$\omega^{\text{C}}_{\text{LO}}(\mathrm{cm}^{-1}) = 628.0(\pm 1.0) + 80.6(\pm 115.4)x \qquad (3)$$

in $x(y'x'+y'z')\bar{x}$ polarization and

$$\omega^{\text{C}}_{\text{TO}}(\mathrm{cm}^{-1}) = 636.8(\pm 1.4) - 0.3(\pm 136.9)x \qquad (4)$$

in $x(y'z')\bar{x}$ polarization. In this case the ''TO'' peak lies at a higher frequency than the ''LO'' peak, which is not the expected relationship for TO-LO pairs. This together with the flat x dependence immediately suggests that the $630\ \mathrm{cm}^{-1}$ band does not correspond to a normal lattice mode of the mixed crystal. For comparison, Finkman *et al.*[14,16] found for a satellite peak near this frequency in $Si_{0.9-x}C_xGe_{0.1}$ that $\omega_{\text{SiCGe}}(\mathrm{cm}^{-1}) = 627.4 + 354x$, corresponding to a much steeper increase with x.

The 605 and $630\ \mathrm{cm}^{-1}$ bands show a similar increase in linewidth with increasing x for both polarizations (see Fig. 5). The band areas (integrated intensities), however, show some differences: The linear increase in the $605\ \mathrm{cm}^{-1}$ band area with increasing x (also reported by Tsang *et al.*[6]) is much greater (by a factor of 3.8) than the linear increase in the $630\ \mathrm{cm}^{-1}$ band area for $x(y'y'+y'z')\bar{x}$ polarization, and also for $x(y'z')\bar{x}$ polarization (here the ratio of slopes was 9.2).

In earlier Raman studies of $Si_{1-x}C_x$ (and $Si_{1-x-y}C_xGe_y$) the $630\ \mathrm{cm}^{-1}$ satellite band has been variously attributed to interstitial C and to pairs of C atoms located on third-nearest-neighbor substitutional sites.[8,14,16,30] In cases where samples were grown by conventional solid-source MBE, this feature has been shown[8,14,16,31] to follow the calculated[8] behavior for third-nearest-neighbor C-C pairs, which are a result of an ordered phase appearing at higher C concentrations.[21] The same ordered C-C mode was found in rapid thermal chemical vapor deposition (RTCVD) grown layers of $Si_{1-x-y}C_xGe_y$.[14,16] On the other hand, for $Si_{1-x-y}C_xGe_y$ samples grown by pulsed laser induced epitaxy,[32] no satellite peak was observed.[14] Clearly, pronounced differences in the

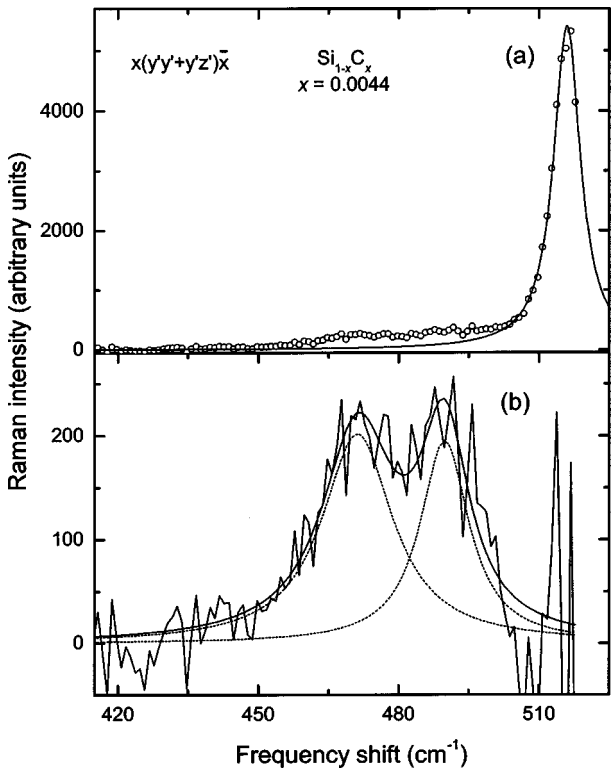

FIG. 6. Curve-resolved $Si_{1-x}C_x$ (x=0.0044) Raman spectra in $x(y'y'+y'z')\bar{x}$ polarization showing fits to (a) the strong Si-Si band plus (b) two weaker side bands.

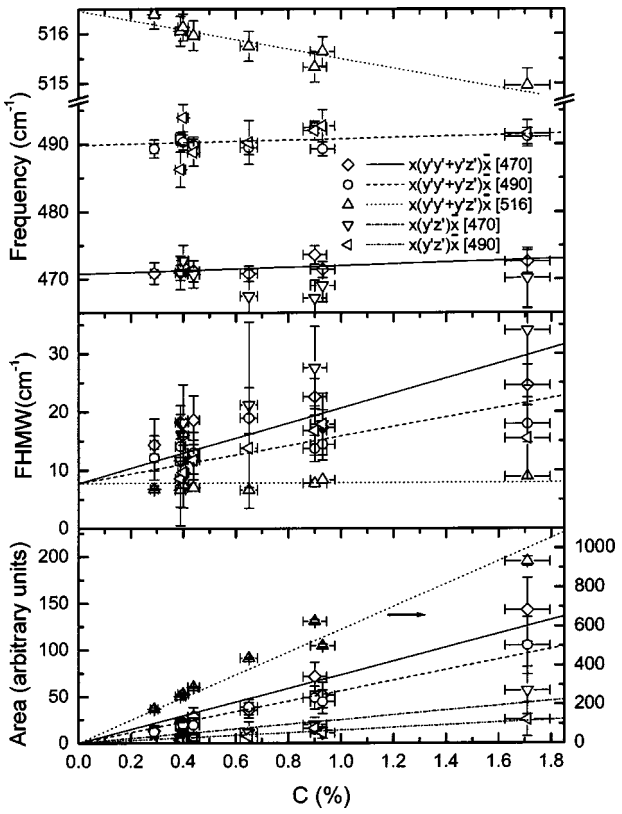

FIG. 7. Concentration dependence of the band parameters for the Si-Si Raman line and its two satellites.

microscopic structure of alloys can result from different growth techniques and different growth rates.[14] In our case, a satellite band is detected near 630 cm^{-1}, but its frequency does not vary with concentration, contrary to what was observed for C-C pair ordering.[14,16] Also, the band intensity grows much too slowly with increasing concentration: Much less than the 605 cm^{-1} band and not in the nonlinear fashion expected for an ordered C-C pair.[16] We conclude that under our plasma-assisted MBE growth conditions this satellite band is not due to C ordering. The 630 cm^{-1} band is seen in all samples except for two of low C concentration ($x=0.0026$ and 0.0039). Also the SIMS-HRXRD comparison (Fig. 1) indicates that not all C atoms are incorporated on Si lattice sites, and this is especially noticeable at higher C concentrations. Thus, we believe that the pair of $\sim$630 cm^{-1} bands originate primarily (i.e., allowing for the possibility of the formation some C-C ordered pairs) from C atoms located on interstitial (defect) sites in the Si lattice where changes in the C concentration (at least for low x values) will not greatly affect the defect mode vibrational frequency. A theoretical investigation by Tersoff of C defects in Si using an empirical classical potential model has shown that substitutional C reacts with Si interstitials, resulting in the C being ''kicked out'' to form a (100) split interstitial.[32] Such a mechanism has been observed previously[33] and was surmised to explain strain compensation in $Si_{1-x-y}C_xGe_y$ layers prepared by ion implantation and laser annealing.[30] Calculations[34] of the dynamical properties of interstitial C and C-C pair defects in Si indicate for one configuration a localized vibrational mode of C at 649 cm^{-1} that is comparable in frequency to the mode observed here, but at this stage the agreement may simply be fortuitous as the precise structure of the C defect in our samples is not known.

B. First-order modes—500 cm^{-1} region

Three Raman bands are observed in this frequency region: A strong band near 516 cm^{-1} and two much weaker bands near 470 and 490 cm^{-1} (see Fig. 6). The band parameters are plotted as a function of x in Fig. 7.

Compared with the two first-order Raman bands discussed earlier, the 516 cm^{-1} band notably decreases in frequency with increasing C concentration:

$$\omega_{LO}^{Si\text{-}Si}(cm^{-1}) = 516.5(\pm 0.2) - 96.5(\pm 25.9)x. \qquad (5)$$

A separate TO-polarized component of this band could not be resolved in these measurements. By analogy with the $Si_{1-y}Ge_y$ alloy where three groups of first-order modes are observed, one would expect for the $Si_{1-x}C_x$ alloy system that the Si-Si, Si-C, and C-C modes should mimic the $Si_{1-y}Ge_y$ behavior. In $Si_{1-y}Ge_y$, the Si-Si (Ge-Ge) mode increases (decreases) in frequency with increasing y.[35] Thus in $Si_{1-x}C_x$, the Si-Si mode, which would correspond to the Ge-Ge mode in $Si_{1-y}Ge_y$, could be expected to decrease in frequency with increasing x starting from $\omega_{LO}^{Si\text{-}Si}=520$ cm^{-1} (the bulk Si value) at $x=0$. This, within error (it is difficult to distinguish experimentally the $\omega_{LO}^{Si\text{-}Si}$ band from the bulk Si

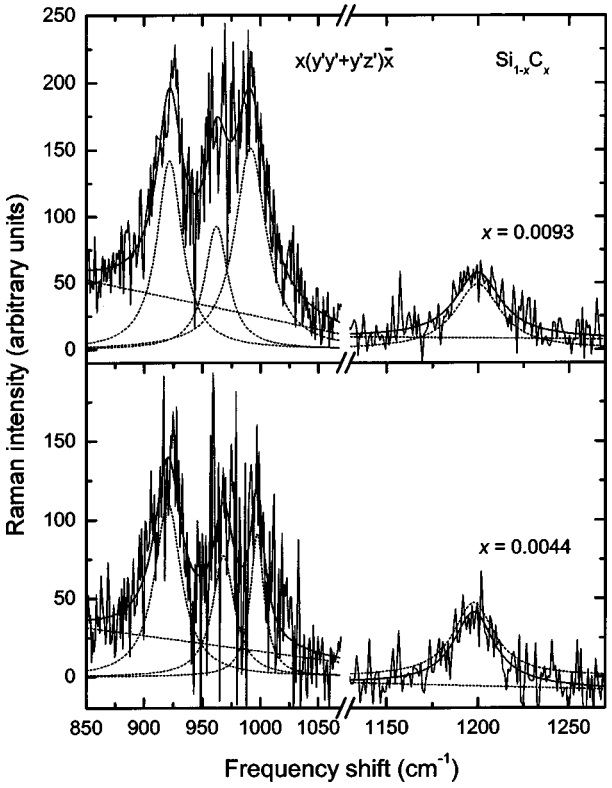

FIG. 8. Multiband fits to the second-order Raman spectrum of $Si_{1-x}C_x$ recorded in $x(y'y'+y'z')\bar{x}$ polarization.

substrate band at very low x values), is what is observed for the 516 cm^{-1} band, confirming the assignment. The C-C mode, however, would be expected to be at much higher frequency and increase in frequency with increasing x. No evidence of this mode was seen in our Raman measurements, owing to the low C carbon concentration. The 516 cm^{-1} band remains sharp, as expected for a first-order band, but its intensity increases in linear fashion with increasing x (see Fig. 7).

The other two bands in this frequency region exhibit essentially no TO-LO splitting and their frequencies increase only slightly with x:

$$\omega_{\mathrm{LO}}(x) = 470.7(\pm 0.9) + 126.9(\pm 123.1)x, \tag{6}$$

$$\omega_{\mathrm{LO}}(x) = 489.9(\pm 0.8) + 95.0(\pm 93.5)x. \tag{7}$$

Their linewidths noticeably increase with x as do their intensities, with the TO modes being three times weaker than the LO modes. The band at 470 cm^{-1} has been observed previously and was assigned originally to disorder induced first-order Raman scattering due to the C mass defect.[17] More recent Raman work[6] has shown that this band is associated with Si lattice relaxation about substitional C sites. The weak dependence of the mode frequency on x shown in Fig. 7 confirms the suggestion[6] that the vibrational excitations of the Si atoms next to substitional C atoms can be localized. The 490 cm^{-1} band was noted earlier by Rücker *et al.*,[8] but no spectrum was given. This band has a similar concentration dependence (see Fig. 7) and hence a similar origin as the

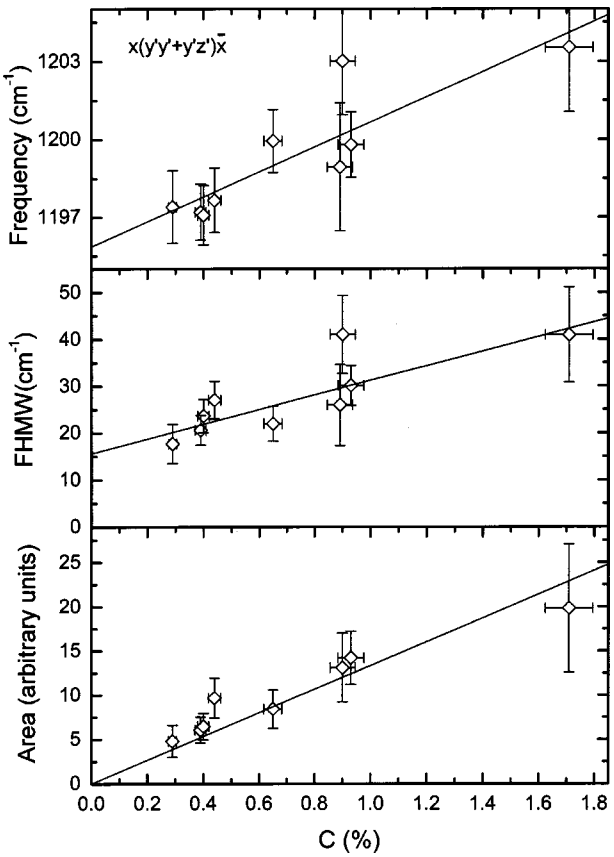

FIG. 9. Concentration dependence of the band parameters of the Si-C second-order Raman line.

470 cm^{-1} band. The phonon calculations of Rüker *et al.*[8] based on an anharmonic Keating model confirm that these two peaks are indeed Si-Si type modes related to the softening of the stretched Si-Si bonds near the substitutional C atom.

C. Second-order bands

The weak feature near 1200 cm^{-1} in $x(y'y'+y'z')\bar{x}$ polarization (see Fig. 8) exhibits a linear increase in all band parameters with increasing C concentration, as shown in Fig. 9. A least-squares fit to the band frequency versus x gives

$$\omega_{2\mathrm{LO}}^{\mathrm{Si\text{-}C}}(\mathrm{cm}^{-1}) = 1195.9(\pm 0.9) + 481.1(\pm 103.8)x. \tag{8}$$

This band was seen by Tsang *et al.*[6] in their Raman study of $Si_{1-x}C_x$ and assigned to overtone Raman scattering. Comparison of Figs. 5 and 9 confirms that it is indeed the second-order equivalent of the $\omega_{\mathrm{LO}}^{\mathrm{Si\text{-}C}}$ peak: The 1200 cm^{-1} band frequency is twice that of $\omega_{\mathrm{LO}}^{\mathrm{Si\text{-}C}}$ and its frequency increases with x at twice the rate of $\omega_{\mathrm{LO}}^{\mathrm{Si\text{-}C}}$ [compare Eqs. (1) and (8)]. Furthermore, the 1200 cm^{-1} band linewidth, although about twice as wide as the 605 cm^{-1} band, increases with x in the same way as the 605 cm^{-1} band and the intensities of both bands increase linearly with x.

Three weak Raman peaks are observed in the 900–1000 frequency range (see Fig. 8) with the center band weaker than the other two. These bands have not been reported be-

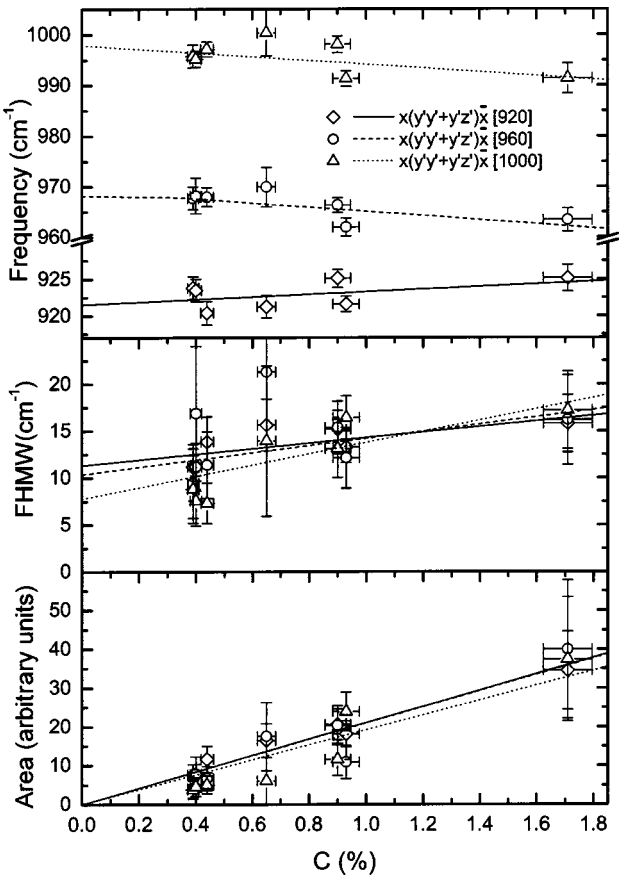

FIG. 10. Concentration dependence of the band parameters of the Si-Si second-order Raman lines.

fore. The band parameters are given as a function of x in Fig. 10. Interestingly, the frequencies of two of the bands *decrease* with increasing x while the other *increases*. Fits to the frequencing data for each band yield

$$\omega_{\mathrm{LO}}(\mathrm{cm}^{-1}) = 921.5(\pm 1.2) + 177.0(\pm 145.2)x, \quad (9)$$

$$\omega_{\mathrm{LO}}(\mathrm{cm}^{-1}) = 969.2(\pm 1.8) - 413.7(\pm 200.2)x, \quad (10)$$

$$\omega_{\mathrm{LO}}(\mathrm{cm}^{-1}) = 997.8(\pm 1.6) - 367.4(\pm 203.7)x. \quad (11)$$

The band linewidths increase slightly with x and their intensities increase linearly with x. From their frequencies, these bands can be assigned to combination bands of the strong first-order Si-Si Raman line at 516 cm^{-1} together with the weaker side bands to lower frequency. Combinations of the 516 cm^{-1} band with itself and the 470 and 490 cm^{-1} bands will produce two-phonon bands that decrease in frequency with increasing x, as in Eqs. (10) and (11). Combinations of the 470 and 490 cm^{-1} bands could produce bands that increase in frequency with x, as in Eq. (9). There are quite a number of possible combination bands and thus the second-order Raman scattering in the 900–1000 cm^{-1} region is only approximately represented by the curve resolving into three bands shown in Fig. 8.

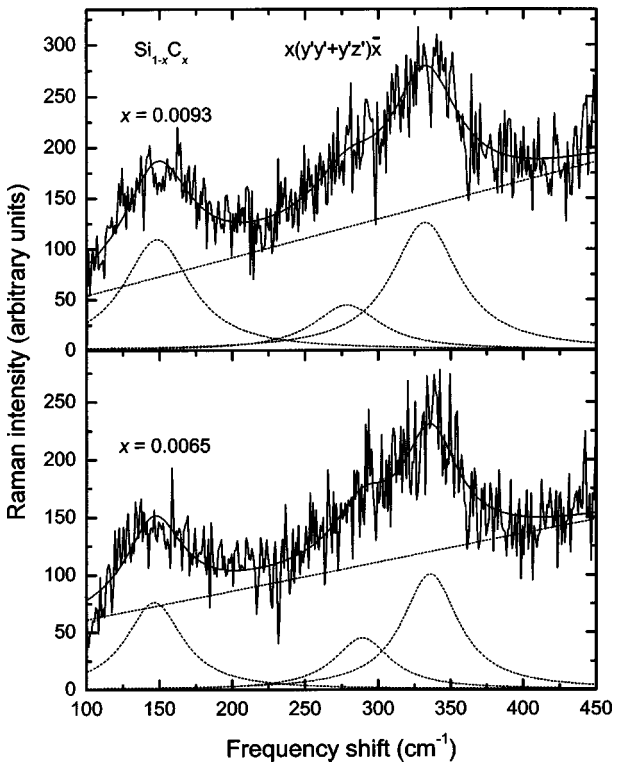

FIG. 11. Multiband fits to the disorder-induced Raman spectrum of $Si_{1-x}C_x$ recorded in $x(y'y'+y'z')\bar{x}$ polarization.

D. Disorder induced bands

In $Si_{1-y}Ge_y$ alloys disorder-induced Raman scattering from acoustic modes is observed at lower frequencies,[36] but no such peaks were found in earlier work on $Si_{1-x}C_x$ alloys.[6] In this study, several peaks were observed in the low frequency Raman spectrum, as shown in Fig 2; curve resolving revealed three bands in $x(y'y'+y'z')\bar{x}$ polarization (see Fig. 11) and one band in $x(y'z')\bar{x}$ polarization. The concentration dependences of the fitted parameters for these four bands are given in Fig. 12. The frequencies of these bands vary as

$$\omega_{\mathrm{LO}}(\mathrm{cm}^{-1}) = 339.1(\pm 1.9) - 761.1(\pm 293.5)x, \quad (12)$$

$$\omega_{\mathrm{LO}}(\mathrm{cm}^{-1}) = 287.1(\pm 5.1) - 636.5(\pm 916.7)x, \quad (13)$$

$$\omega_{\mathrm{LO}}(\mathrm{cm}^{-1}) = 143.8(\pm 1.5) + 297.2(\pm 152.6)x, \quad (14)$$

$$\omega_{\mathrm{TO}}(\mathrm{cm}^{-1}) = 133.8(\pm 3.2) + 273.2(\pm 354.8)x. \quad (15)$$

The first two bands decrease in frequency with increasing x while the other two increase in frequency. The bands are broad, which is typical of disorder-induced acoustic mode scattering, and widen appreciably with increasing x. The band integrated intensities increase nonlinearly with x at higher C concentrations (the fits shown in Fig. 12 for the 135, 145, and 340 cm^{-1} bands are for an exponential increase in the area). This rapid increase in intensity is also consistent with disorder activated Raman modes. The TO-LO pair near 135 and 145 cm^{-1} arises most likely from transverse acoustic modes, while the higher frequency bands

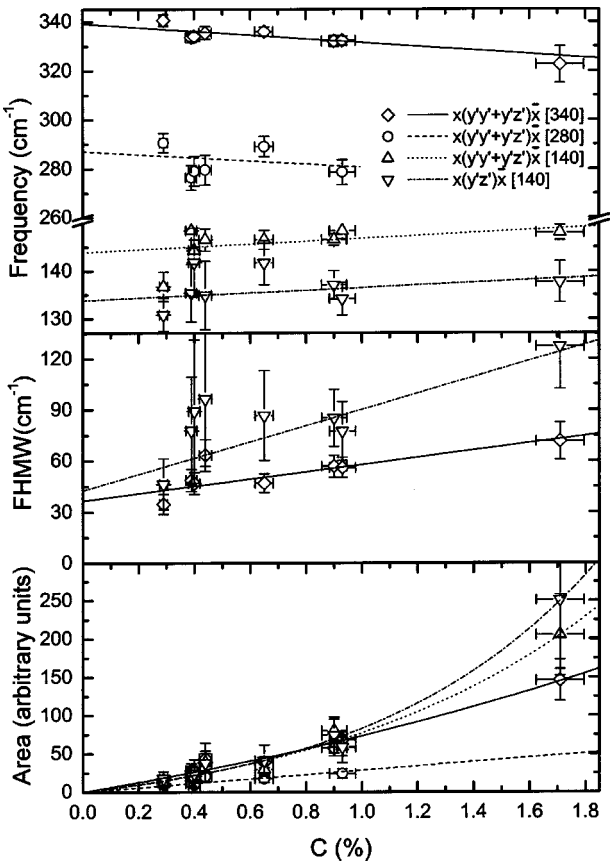

FIG. 12. Concentration dependence of the band parameters of the disorder-induced Raman lines.

could be associated with longitudinal acoustic modes, at wave vectors near the Brillouin zone boundary.

E. Optical absorption in $Si_{1-x}C_x$

For uncapped $Si_{1-x}C_x$ samples, it is possible to evaluate the optical absorption near the laser wavelength of 457.9 nm from a measurement of the intensity of the Si substrate Raman line at 520 cm^{-1} normalized to that of a reference Si wafer. If α is the optical absorption coefficient, then as both the incident (exciting) laser light (α_i) and the back scattered Raman light at 520 cm^{-1} shift or 469.1 nm in wavelength (α_s) have to traverse the $Si_{1-x}C_x(100)$ layer of thickness d, the Si substrate Raman intensity $I \propto \exp\text{-}(\alpha_i+\alpha_s)d$. In crystalline Si, $\alpha_i = 3.57\ \mu\text{m}^{-1}$ at 457.9 nm and $\alpha_s = 3.68\ \mu\text{m}^{-1}$ at 469.1 nm,[37] and the average value $\alpha = 3.625$ is thus one end point ($x=0$) for $Si_{1-x}C_x$ on Si(100). The correction for the film contribution to the total Raman intensity at 520 cm^{-1} is small for the layer thicknesses studied here (see Fig. 6) and

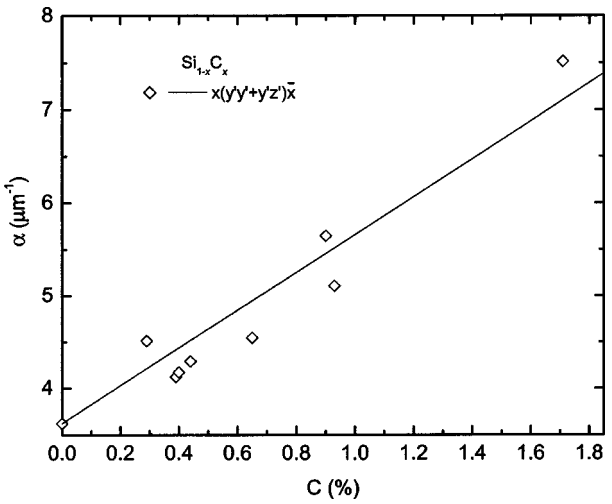

FIG. 13. Concentration dependence of the optical absorption coefficient α of $Si_{1-x}C_x$ near 458 nm for $x(y'y'+y'z')\bar{x}$ polarization.

can be neglected. Figure 13 shows the variation in α deduced from the Si 520 cm^{-1} Raman line intensity in each uncapped $Si_{1-x}C_x$ sample. Allowing for the uncertainty in the data, the absorption coefficient increases approximately linearly and also steeply with increasing C concentration over the x range studied here.

V. CONCLUSIONS

This detailed experimental investigation by Raman spectroscopy of the lattice vibrations of $Si_{1-x}C_x$ epilayers on Si(100) for $0<x<0.02$ has revealed a complex and rich behavior, even for such low concentrations of C. Two of the three expected main first-order peaks have been observed together with two weaker satellite bands associated with local lattice distortions. Their band frequencies all exhibit a linear variation with C concentration. A number of second-order Raman bands have been discovered that are related to the first-order bands. Disorder induced Raman scattering from acoustic modes shows a strong dependence on the C concentration, as does the optical absorption near 458 nm. The results show that the addition of only a relatively small amount of C strongly perturbs the Si lattice, affecting considerably the vibrational and optical properties.

ACKNOWLEDGMENTS

We thank Robin Radomski for assistance in the preliminary Raman data analysis and S.J. Rolfe for the SIMS measurements. H.X. Xu is grateful for support from Chalmers University of Technology.

*Present address: Department of Applied Physics, Chalmers University of Technology, Sweden.

[1] *Properties of Silicon Germanium and SiGe: Carbon*, edited by E. Kasper and K. Lyutovich (IEE, Stevenage, 2000).

[2] S.S. Iyer, K. Eberl, M.S. Goorsky, F.K. LeGoues, J.C. Tsang, and F. Cardone, Appl. Phys. Lett. **60**, 356 (1992).

[3] K. Eberl, O.G. Schmidt, and R. Duschl, in *Properties of Silicon Germanium and SiGe: Carbon* (Ref. 1), p. 75.

[4] D.J. Lockwood and J.-M. Baribeau, Phys. Rev. B **45**, 8565 (1992).

[5] K. Brunner, in *Properties of Silicon Germanium and SiGe: Carbon* (Ref. 1), p. 115.

[6] J.C. Tsang, K. Eberl, S. Zollner, and S.S. Iyer, Appl. Phys. Lett. **61**, 961 (1992).
[7] S.C. Jain, H.J. Osten, B. Dietrich, and H. Rücker, Semicond. Sci. Technol. **10**, 1289 (1995).
[8] H. Rücker, M. Methfessel, B. Dietrich, K. Pressel, and H.J. Osten, Phys. Rev. B **53**, 1302 (1996).
[9] K. Eberl, S.S. Iyer, S. Zollner, J.C. Tsang, and F.K. LeGoues, Appl. Phys. Lett. **60**, 3033 (1992).
[10] B. Dietrich, H.J. Osten, H. Rücker, M. Methfessel, and P. Zaumseil, Phys. Rev. B **49**, 17 185 (1994).
[11] H. Rücker, M. Methfessel, B. Dietrich, H.J. Osten, and P. Zaumseil, Superlattices Microstruct. **16**, 121 (1994).
[12] J. Menéndez, P. Gopalan, G.S. Spencer, N. Cave, and J.W. Strane, Appl. Phys. Lett. **66**, 1160 (1995).
[13] M. Melendez-Lira, J. Menéndez, W. Windl, O.F. Sankey, G.S. Spencer, S. Sego, R.B. Culbertson, A.E. Blair, and T.L. Alford, Phys. Rev. B **54**, 12 866 (1996).
[14] E. Finkman, H. Rücker, F. Meyer, S.D. Prower, D. Bouchier, J. Boulmer, S. Bodnar, and J.L. Regolini, Thin Solid Films **292**, 118 (1997).
[15] C. Guedj, X. Portier, A. Hairie, D. Bouchier, G. Calvarin, and B. Piriou, Thin Solid Films **294**, 129 (1997).
[16] E. Finkman, F. Meyer, and M. Mamor, J. Appl. Phys. **89**, 2580 (2001).
[17] R. Forman, M. Bell, D. Meyers, and D. Chandler-Horowitz, Jpn. J. Appl. Phys. **10**, L848 (1985).
[18] R. Newman and R. Smith, J. Phys. Chem. Solids **30**, 1493 (1969).
[19] J.W. Strane, H.J. Stein, S.R. Lee, S.T. Picraux, J.K. Watanabe, and J.W. Mayer, J. Appl. Phys. **76**, 3656 (1994).
[20] K. Pressel, G.G. Fischer, P. Zaumseil, M. Kin, and H.J. Osten, Thin Solid Films **294**, 133 (1997).
[21] H. Rücker, M. Methfessel, E. Bugiel, and H.J. Osten, Phys. Rev. Lett. **72**, 3578 (1994).
[22] J.-M. Baribeau, D.J. Lockwood, M.W.C. Dharma-wardana, N.L. Rowell, and J.P. McCaffrey, Thin Solid Films **183**, 17 (1989).
[23] J.-M. Baribeau, D.J. Lockwood, J. Balle, S.J. Rolfe, and G.I. Sproule, Mater. Sci. Eng., B **89**, 296 (2002); J.-M. Baribeau, D.J. Lockwood, J. Balle, S.J. Rolfe, G.I. Sproule, and S. Moisa, Thin Solid Films **410**, 61 (2002).
[24] Bede Scientific RADS Mercury software.
[25] P.C. Kelires, Phys. Rev. B **55**, 8784 (1997).
[26] D.J. Lockwood, M.W.C. Dharma-wardana, J.-M. Baribeau, and D.C. Houghton, Phys. Rev. B **35**, 2243 (1987).
[27] M.I. Alonso and K. Winer, Phys. Rev. B **39**, 10 056 (1989).
[28] S. de Gironcoli, Phys. Rev. B **46**, 2412 (1992).
[29] J.A. Baker, T.N. Tucker, N.E. Moyer, and R.C. Buschert, J. Appl. Phys. **39**, 4365 (1968).
[30] A. Grob, J.J. Grob, D. Muller, B. Prévot, R. Stuck, and E. Fogarassy, Thin Solid Films **294**, 145 (1997).
[31] H.J. Osten, D. Endisch, E. Bugiel, B. Dietrich, G.G. Fischer, M. Kim, D. Kruger, and P. Zaumseil, Semicond. Sci. Technol. **11**, 1678 (1996).
[32] J. Tersoff, Phys. Rev. Lett. **64**, 1757 (1990).
[33] G.D. Watkins and K.L. Brower, Phys. Rev. Lett. **36**, 1329 (1976).
[34] P. Leary, R. Jones, S. Öberg, and V.J.B. Torres, Phys. Rev. B **55**, 2188 (1997).
[35] H.K. Shin, D.J. Lockwood, and J.-M. Baribeau, Solid State Commun. **114**, 505 (2000), and references therein.
[36] P. Temple and C. Hathaway, Phys. Rev. B **7**, 3685 (1973).
[37] *Handbook of Optical Constants of Solids*, edited by E.D. Palik (Academic Press, New York, 1985), p. 564.